Mech. Sci., 17, 511–523, 2026
https://doi.org/10.5194/ms-17-511-2026

Mechanical Sciences
Open Access

Optimization of structural process parameters of rod stirring mill based on discrete element method

Zhaoguo Wang[1,2,3] **and Wenlong Chen**[2]

[1]The First Affiliated Hospital of Anhui University of Science and Technology, Huainan 232000, China
[2]Anhui Intelligent Mine Technology and Equipment Engineering Research Center, School of Mechatronic Engineering, Anhui University of Science and Technology, Huainan 232000, China
[3]Hefei Changyuan Hydraulic Co., Ltd., Hefei, 230000, China

Correspondence: Zhaoguo Wang (wangzhaoguosdu@163.com)

Received: 29 September 2025 – Revised: 15 April 2026 – Accepted: 19 April 2026 – Published: 11 May 2026

Abstract. The rod-type stirred mill is the core equipment used in the grinding of potassium feldspar. However, the grinding process involves numerous parameters that influence performance, various evaluation metrics, and prolonged single-cycle durations, collectively making it difficult to identify optimal operating conditions. To address this challenge, a simulation model of the rod-type stirred mill was developed based on the discrete element method (DEM). This study investigates the effects of rotational speed, grinding media size, and bar spacing on milling performance. By integrating energy efficiency, stirrer wear, collision frequency, and average normal and tangential collision forces, the comprehensive index of milling performance was established. Using Box–Behnken experimental design and analysis of variance, the relative influence of rotational speed, grinding media size, and bar spacing on grinding performance was ranked. With weight coefficients assigned as 0.4 for energy efficiency, 0.2 for stirrer wear, 0.2 for collision frequency, 0.1 for average normal collision force, and 0.1 for average tangential collision force, response surface optimization was conducted. Under the current weighting scheme, the optimal operating parameters of the rod-type stirred mill are determined as follows: a rotational speed of 398 r min^{-1}, a grinding media size of 6 mm, and bar spacing of 21.2 mm. Under these conditions, the predicted comprehensive grinding performance indicator is 0.781, and the error between the discrete element method (DEM) simulation validation results and the predicted value is only 0.77 %.

1 Introduction

The stirred rod mill is a fine grinding device (Kumar et al., 2020) that reduces mineral particle size through friction, shear, and compression between the grinding media and the material (Fukui et al., 2018). It offers several advantages, including high grinding efficiency, precise particle size control, energy savings, and strong adaptability (Daraio et al., 2020), and has thus become a key technology for fine and ultrafine grinding of potassium ores (Cleary and Owen, 2019). However, when applied to potassium feldspar, the milling process involves numerous operational variables (Govender et al., 2018), inconsistent performance indicators, and prolonged single-cycle durations – factors that together make it difficult to establish optimal process parameters (Kumar et al., 2023).

The DEM is a commonly used approach in mill research. AmanNejad and Barani (2021) applied DEM to examine the effects of grinding media size distribution, mill speed, and their interaction on horizontal ball mill performance. Bor et al. (2020) used DEM simulations to investigate how grinding media type, rotational speed, and processing time influence the coating characteristics of metal matrix carbon nanotube composites in both conventional and stirred ball mills. Tavares and Das Chagas (2021) proposed a stochastic particle replacement strategy to model breakage in DEM frameworks. Oliveira et al. (2020) developed and validated a DEM-based model of a vertical spiral stirred mill. Barrios et al. (2020) employed a DEM particle replacement model

to simulate particle fragmentation in stirred ball mills. Miao et al. (2024) utilized DEM to analyze impact breakage patterns of individual spherical and ellipsoidal particles in drop-weight tests. Prziwara et al. (2018) examined the effects of grinding aids and process parameters on dry stirred media mills using DEM simulations. Liu et al. (2022) developed a coupled DEM–multibody dynamics model of a laboratory-scale semi-autogenous mill to evaluate its performance under varying operating conditions. Ding et al. (2025) formulated a coupled DEM–CFD model for wet semi-autogenous grinding, enabling comparative analysis of particle motion and collision energy distribution for ores of different grades under both dry and wet conditions. Xie et al. (2022) employed DEM to analyze critical structural and operational parameters of vertical spiral stirred mills, identifying optimal parameter combinations through orthogonal experimental design. Ou et al. (2023) coupled DEM with smoothed particle hydrodynamics to simulate solid–liquid flow based on dynamic free surfaces, applying this approach to quantitatively compare the effects of different mill liner configurations on discharge efficiency.

In summary, existing research has primarily focused on vertical spiral stirred mills, while studies on stirred rod mills remain limited – particularly regarding the influence of structural and process parameters on grinding performance. To address this gap, a simulation model of a stirred rod mill was developed using DEM to investigate the effects of rotational speed, grinding media size distribution, and bar spacing on milling performance. A comprehensive index of milling performance was formulated by integrating energy efficiency, stirrer wear, collision frequency, and average normal and tangential collision forces. Using Box–Behnken experimental design and analysis of variance, the relative significance of the three operational parameters was determined. Response surface optimization was subsequently applied to identify the optimal structural and process parameters for the stirred rod mill.

2 Discrete element simulation of stirring and grinding process

2.1 Establishment of discrete element simulation model

The rod agitator mill consists of an agitator, a cylinder, a driving device and a transmission device. In order to shorten the simulation time, the three-dimensional model is simplified and processed, as shown in Fig. 1, and the related parameters are shown in Table 1.

The grinding media used in the stirred rod mill are steel balls with a Poisson's ratio of 0.3, a density of 7850 kg m^{-3}, a shear modulus of 7.9×10^{10} Pa, and a diameter of 10 mm. The filling rate is set to 60 %. The number of steel balls charged into the mill is calculated using the following formula (De Oliveira et al., 2021):

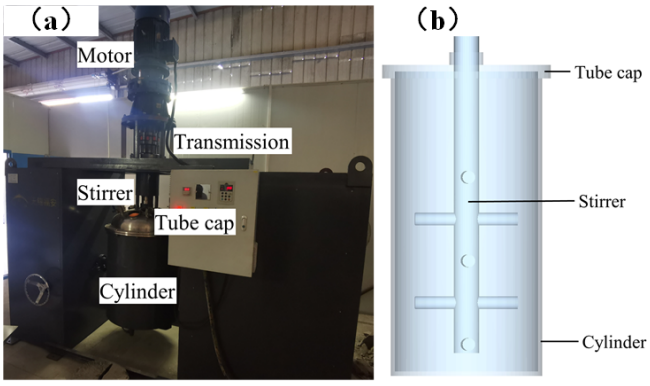

Figure 1. Grinding mill physical object and simplified three-dimensional model: **(a)** the physical diagram of the stirred rod mill and **(b)** the simplified three-dimensional model.

Table 1. Model size.

Parametric	Value
Cylinder outer diameter (mm)	180
Inside diameter of cylinder (mm)	170
Cylinder height (mm)	360
Agitator shaft diameter (mm)	30
Stirrer track diameter (mm)	122
Rod length (mm)	61
Rod diameter (mm)	15
Bar spacing (mm)	35
Number of rods (root)	5
Distance between the bottom of the agitator and the bottom of the barrel (mm)	22

$$N = 1.2\frac{m/\rho}{V_0} \cdot \frac{1}{1-\xi} \cdot V_0/d^3, \tag{1}$$

where m is the total mass of the grinding media, ρ is the density of the media, V_0 is the effective volume of the drum, ξ is the void fraction (taken as 0.4), and d is the inner diameter of the drum.

Based on Eq. (1), the mill is charged with 5573 grinding media balls. The Hertz–Mindlin (no-slip) model is employed for particle–particle contacts, and the Archard wear model is adopted for particle–geometry interactions (Mittal et al., 2024). The simulation parameters are summarized in Table 2.

2.2 Analysis of discrete element simulation results

Figure 2a presents the velocity distribution of the grinding media during stirred rod mill operation. In the vicinity of the

Table 2. Simulation parameter setting.

Parameters	Value	Parameters	Value
Rotational speed (r min^{-1})	300	Coefficient of restitution	0.6
Simulation duration (s)	5	Coefficient of static friction	0.5
Simulation step (%)	20	Coefficient of rolling friction	0.03

stirrer's rotational axis, the media exhibit relatively low velocities. As radial distance increases, the velocity rises progressively, peaking at the outer tips of the stirring rods. Beyond this region, the velocity declines toward the inner wall of the drum, while the velocity field between adjacent stirring rods remains comparatively uniform. The tangential velocity distribution in Fig. 2b reveals that the outer ends of the stirring rods are where the grinding media move most rapidly, identifying this region as the zone of optimal grinding efficiency. The vertical velocity distribution in Fig. 2c indicates that the grinding media move more rapidly above the stirring rods than below them. This pattern arises because, during operation, the media are driven upward by the rods, after which they descend under gravity upon encountering subsequent rods, thereby establishing a stable recirculating flow.

Figure 3 illustrates the pressure distribution on the surface of the stirred rod mill. The pressure at the outer ends of the lower stirring rods is higher than that at the upper rods, with elevated pressure also observed at the bottom and side walls of the drum. Additionally, pressure in the peripheral regions of the drum is lower than in the central zone. The gradual decrease in pressure from the lower to the upper rod ends is due to the vortex formed by the grinding media during stirrer operation, which subjects the lower rods to greater load than the upper ones.

Figure 4 presents the wear distribution of the stirred rod mill. Wear is predominantly concentrated at the outer ends of the stirring rods, with the lower rods exhibiting greater wear than the upper ones. This pattern results from the vortex formed by the grinding media as driven by the stirrer, which leads to more frequent contact between the lower rods and the media, accompanied by elevated pressure in that region.

3 Influence of different parameters on the grinding process

3.1 Influence of rotational speed on grinding performance

To investigate the effect of rotational speed on grinding performance, motor rotational speeds of 200, 250, 300, 350, and 400 r min^{-1} were selected for simulation. As shown in Fig. 5, both power and torque increase with rising speed, accompanied by a marked acceleration in power consumption. This trend is attributed to intensified collisions between the grinding media and the stirrer at higher speeds, which increase the mechanical load. Consequently, to reduce energy consumption while fulfilling operational requirements, a lower rotational speed is preferable.

Figure 6 presents the vertical force and wear of the stirrer as functions of rotational speed. Wear increases with rising speed, while the vertical force gradually declines. This behavior is attributed to the increased centrifugal force acting on the grinding media at higher speeds. When this centrifugal force exceeds the combined gravitational and internal frictional forces, the media are propelled toward the drum wall, forming an annular layer. As a result, the frequency of vertical contact between the stirrer and the media decreases, the axial compression effect weakens, and the vertical force is reduced. Concurrently, higher rotational speed accelerates the relative motion between the grinding media and the stirrer, intensifying their interaction and thereby exacerbating wear.

Figure 7 shows the variation in the average normal and tangential collision forces of the grinding media with rotational speed. Both forces increase as the stirrer speed rises, due to more intense relative motion among the media particles, which amplifies collision forces. In addition, the average normal collision force increases at a faster rate than the tangential component. This difference arises because, at higher speeds, media particles tend to undergo more frontal or near-frontal impacts, making the normal force the dominant factor in inter-particle collisions.

Figure 8 illustrates the variation in collision frequency and single collision energy of the grinding media with rotational speed. As the stirrer speed increases, the collision frequency declines. This trend is attributed to the growing dominance of centrifugal force, which drives the media toward the drum wall and forms a stable annular flow layer. Under these conditions, the direct driving effect of the stirrer on the media is reduced, leading to fewer inter-particle collisions. Conversely, the single collision energy rises with increasing speed, resulting from the greater drop height of the media and the correspondingly higher impact velocity at the moment of collision.

3.2 Influence of grinding media size on grinding performance

Figure 9 presents the effect of grinding media size on power and torque. Both power and torque increase with larger media diameters, as a greater grinding media size requires

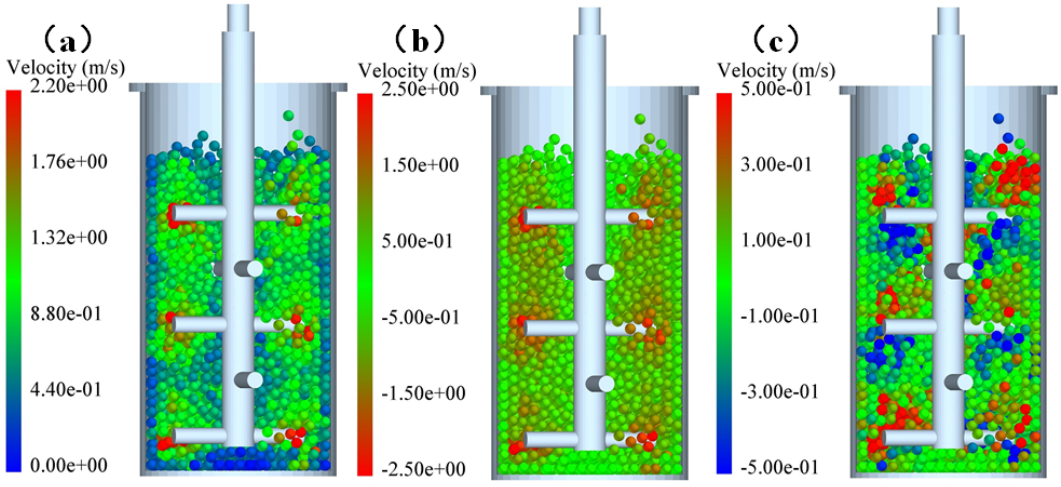

Figure 2. Velocity distribution of grinding media: **(a)** resultant velocity, **(b)** tangential velocity, and **(c)** vertical velocity.

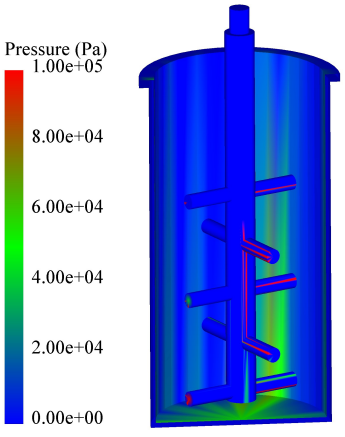

Figure 3. Pressure distribution.

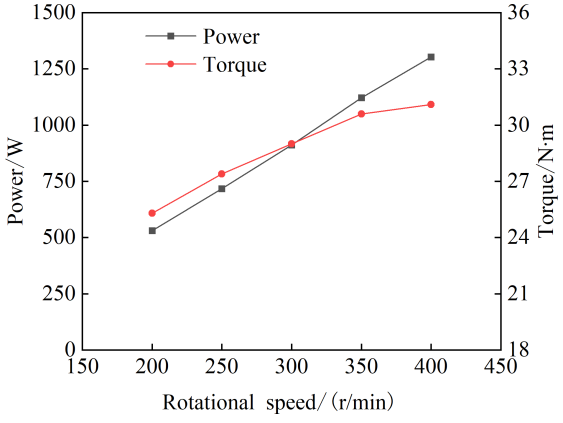

Figure 5. Effect of rotational speed on power and torque.

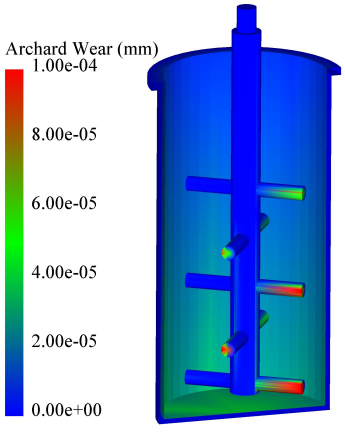

Figure 4. Distribution of stirring wear.

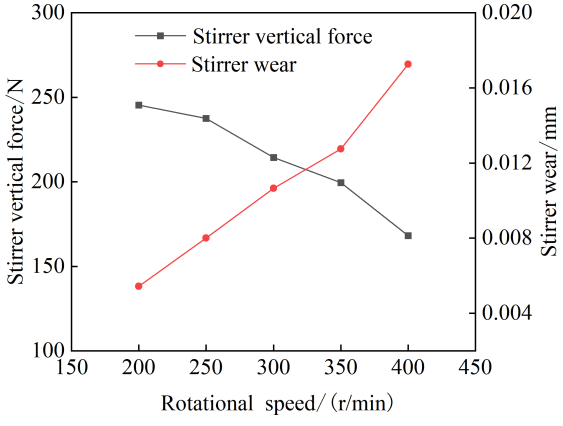

Figure 6. Effect of rotational speed on stirrer vertical force and stirrer wear.

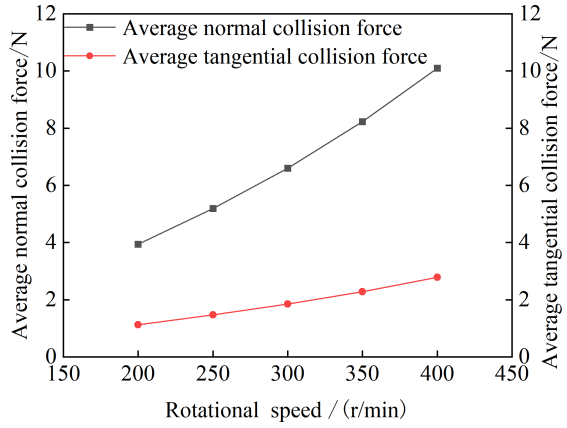

Figure 7. Effect of rotational speed on average normal and tangential collision forces.

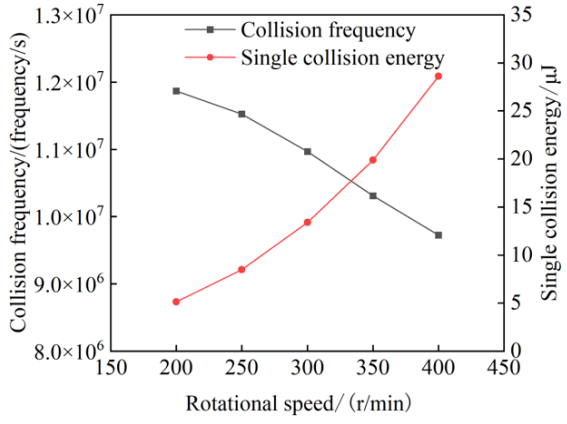

Figure 8. Effect of rotational speed on collision frequency and single collision energy.

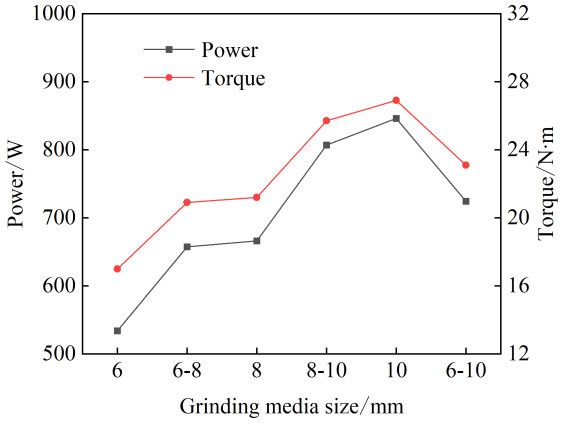

Figure 9. Effect of grinding media size on power and torque.

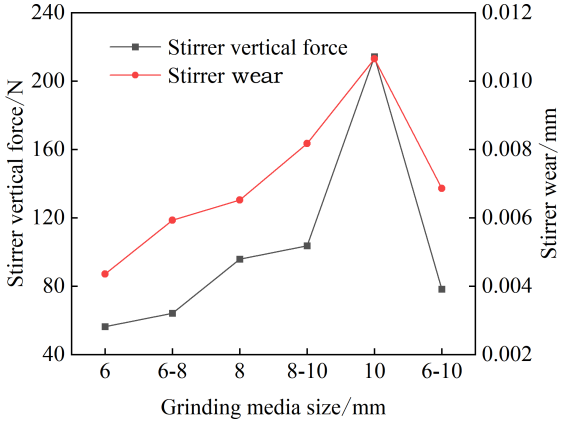

Figure 10. Effect of grinding media size on stirrer vertical force and stirrer wear.

higher power and torque input, leading to increased energy consumption.

Figure 10 shows the variation in vertical force and stirrer wear with grinding media size. For both single-sized and mixed-sized media, vertical force and wear increase as grinding media size increases.

Figure 11 illustrates the variation in average normal and tangential collision forces with grinding media size. For both single-sized and mixed-sized media, the collision forces increase as the media diameter increases. However, as the size range broadens, the collision force first increases and then decreases. The reduction observed for the 6–10 mm size distribution is attributed to the diminished impact effectiveness of smaller media when interacting with larger particles or coarser media. In such cases, energy transfer efficiency is insufficient to generate the required breakage force. Consequently, for grinding coarse materials, selecting larger media is more effective in transmitting energy and achieving the necessary collision force.

Figure 12 illustrates the variation in collision frequency and single collision energy with grinding media size. As media diameter increases, collision frequency decreases progressively, while single collision energy increases. For mixed-size media, as the size distribution broadens, collision frequency initially decreases and then increases, and single collision energy follows the opposite trend – first increasing and then decreasing. Nevertheless, the overall trend indicates a net reduction in collision frequency and a net increase in single collision energy as the size range expands.

3.3 Influence of stir bar spacing on grinding performance

Figure 13 illustrates the variation in power and torque as functions of stirring bar spacing. Both power and torque initially increase and then decrease with increasing bar spacing. The maximum values are observed at a spacing of 25 mm, while the minimum occurs at 35 mm. At smaller spacings, the grinding media become densely packed between the rods, resulting in restricted mobility and a substantial increase in

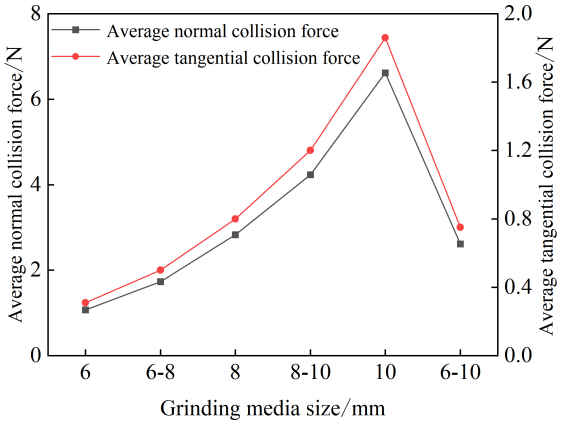

Figure 11. Effect of grinding media size on average normal and tangential collision forces.

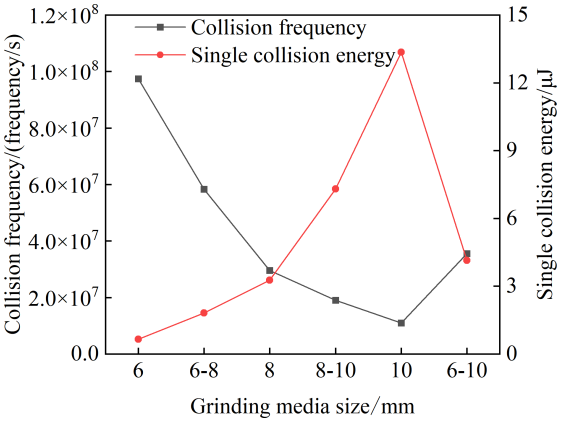

Figure 12. Effect of grinding media size on collision frequency and single collision energy.

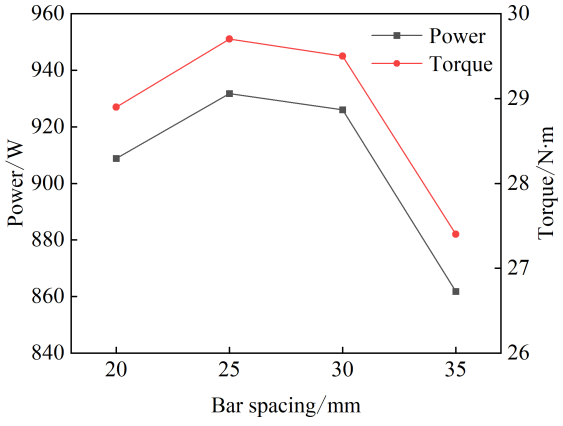

Figure 13. Effect of bar spacing on power and torque.

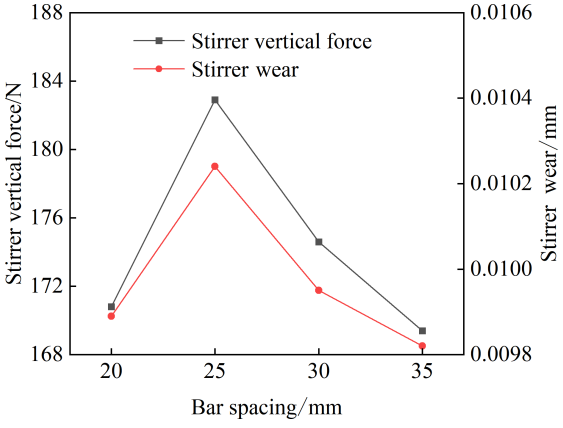

Figure 14. Effect of bar spacing on stirrer vertical force and stirrer wear.

inter-particle normal and tangential forces. This condition requires the stirrer to expend additional energy to overcome the congested region, leading to a marked rise in power draw and torque. As bar spacing increases, the free flow space among particles expands, and inertial forces become dominant. The reduced frequency of particle–stirrer contact lowers energy transfer efficiency, causing power draw and torque to decline. Therefore, the appropriate selection of bar spacing is critical for optimizing the power consumption of the stirrer.

Figure 14 presents the vertical force acting on the stirrer and the corresponding wear profile as functions of bar spacing. Both variables initially increase and then decrease as bar spacing widens. At smaller spacings, the confined particle movement leads to more frequent and intense collisions between particles and stirring rods, thereby increasing the vertical pressure on the stirrer. Concurrently, elevated inter-particle friction and shear forces intensify stirrer wear. As bar spacing increases, the available space for particle motion expands, reducing the number of particles affected by each rod. The relative motion among particles becomes looser, and the frequency of collisions and friction gradually declines, resulting in a decrease in both vertical force and wear.

Figure 15 shows the average normal and tangential collision forces of the grinding media as functions of bar spacing. Both forces first increase with bar spacing, reach a maximum at 25 mm, and then decrease. At smaller spacings, confined particle motion disperses collision energy, leading to lower forces. A moderate increase in spacing provides particles with a longer acceleration path, substantially enhancing kinetic energy and thereby raising collision forces. Excessive spacing, however, reduces the effective driving region of the rods; particles further from the rods decelerate, and collisions become dominated by gravity and random flow, causing both normal and tangential forces to decline.

Figure 16 illustrates the effect of bar spacing on collision frequency and single collision energy. These two parameters exhibit opposing trends as bar spacing increases. Initially, greater spacing leads to more dispersed relative motion among particles, reducing collision frequency. At this stage, the average relative normal collision velocity between adjacent particles rises, thereby increasing the single collision en-

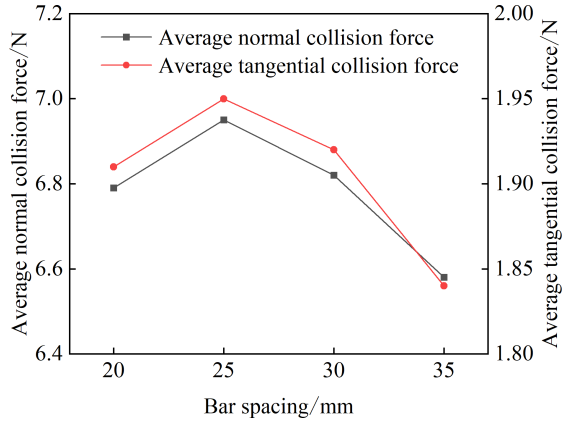

Figure 15. Effect of bar spacing on average normal and tangential collision forces.

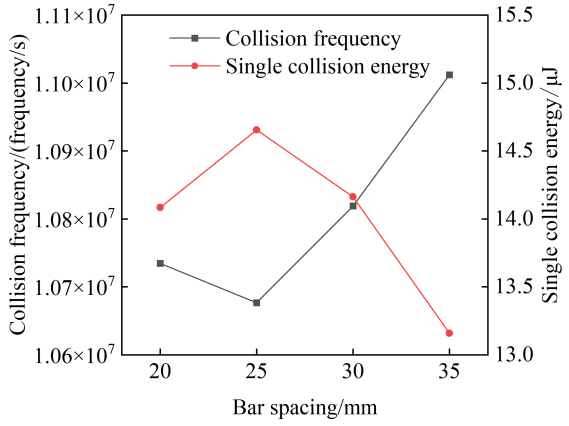

Figure 16. Effect of bar spacing on collision frequency and single collision energy.

ergy. However, as bar spacing continues to increase, particle collisions become governed primarily by gravity and random flow rather than active acceleration by the stirring rods. Consequently, after peaking, the single collision energy gradually declines. Meanwhile, complex recirculating flow patterns develop within the drum, giving rise to secondary collisions in the central or peripheral regions, which in turn elevate collision frequency.

4 Response surface optimization of structural process parameters of stirred mills

4.1 Experimental objectives

To characterize the grinding performance of the stirred rod mill, a set of evaluation indicators was adopted: energy efficiency (x_1), stirrer wear (x_2), collision frequency (x_3), average normal collision force (x_4), and average tangential collision force (x_5). The corresponding weight coefficients were assigned as 0.4, 0.2, 0.2, 0.1, and 0.1, respectively (Xie et al., 2024).

The selected indicators are defined as follows: energy efficiency is the ratio of total collision energy to total energy input. It quantifies the effective conversion of input energy and reflects the mill's capacity to transform drive power into useful grinding work. A higher value indicates more effective grinding. Total collision energy is the product of average collision energy and collision frequency. It serves as a key intermediate variable representing the overall grinding intensity; greater total collision energy corresponds to higher grinding intensity. Mill power draw is calculated as the product of torque acting on the stirrer and its angular velocity. Higher power draw is associated with increased grinding efficiency.

Average collision energy is defined as the kinetic energy expended in a collision between two adjacent particles and is calculated as (Xie et al., 2022)

$$\overline{E_i} = \frac{1}{2} m \overline{v_{ij}^2}, \tag{2}$$

where $\overline{v_{ij}}$ is the average relative normal collision velocity between two adjacent grinding media balls.

The reference indicators were normalized as follows. Using energy efficiency as an example, the mean value of this indicator is given by

$$\overline{x_1} = (x_{1,1} + x_{1,2} + \ldots + x_{1,17})/17. \tag{3}$$

Following this procedure, the normalized energy efficiency for each simulation trial is obtained as

$$\overline{x_{1,i}} = \frac{x_{1,i}}{\overline{x_1}}. \tag{4}$$

The comprehensive index of milling performance W_i is defined as

$$W_i = 0.4\overline{x_{1,i}} - 0.2\overline{x_{2,i}} + 0.2\overline{x_{3,i}} + 0.1\overline{x_{4,i}} + 0.1\overline{x_{5,i}}, \tag{5}$$

where stirrer wear is treated as a negative indicator and is therefore assigned a negative sign. A larger value of the comprehensive index of milling performance W_i indicates better milling performance.

4.2 Design of experiments

This study investigates the effects of rotational speed, grinding media size, and bar spacing on the comprehensive index of milling performance. Based on the actual operating conditions of the stirred rod mill investigated in this study, the rotational speed was set within the range of 200–400 r min^{-1}, the grinding media size ranged from 6 to 10 mm, and the bar spacing varied between 20 and 35 mm. The rotational speed (A), grinding media size (B), and bar spacing (C) were coded, and the levels of each factor were set to -1, 0, and 1, as shown in Table 3. The Box–Behnken design matrix and corresponding DEM simulation results are given in Table 4.

Table 3. Experimental factors and levels.

Level	A: rotational speed ($\mathrm{r\,min^{-1}}$)	B: grinding media size (mm)	C: bar spacing (mm)
−1	200	6	20
0	300	8	27.5
1	400	10	35

4.3 Experimental results and analysis

Multiple linear regression equations were fitted using rotational speed (A), grinding media size (B), and bar spacing (C) as independent variables in the response surface analysis. The response variables were energy efficiency (x_1), stirrer wear (x_2), collision frequency (x_3), average normal collision force (x_4), average tangential collision force (x_5), and comprehensive index of milling performance (W). The resulting regression equations are presented below:

$$\begin{aligned} x_1 = {} & 0.000388A + 0.034255B + 0.00402C \\ & + 0.000011AB + 2.82936 \times 10^{-7}AC \\ & - 0.000081BC - 2.3921 \times 10^{-7}A^2 \\ & - 0.001547B^2 - 0.000072C^2 - 0.187638. \end{aligned} \tag{6}$$

$$\begin{aligned} x_2 = {} & -0.000061A - 0.008325B + 0.00022C \\ & + 7.03375 \times 10^{-6}AB + 6.3 \times 10^{-8}AC \\ & - 0.000032BC + 5.9395 \times 10^{-8}A^2 \\ & + 0.000548B^2 - 2.18667 \times 10^{-7}C^2 + 0.034056. \end{aligned} \tag{7}$$

$$\begin{aligned} x_3 = {} & 61253.80442A - 1.21274 \times 10^{8}B \\ & - 1.8149 \times 10^{6}C - 1595.34AB \\ & + 247.77767AC + 44691.1BC \\ & - 111.77725A^2 + 6.18564 \times 10^{6}B^2 \\ & + 14685.01289C^2 + 6.21322 \times 10^{8}. \end{aligned} \tag{8}$$

$$\begin{aligned} x_4 = {} & -0.049612A - 4.82815B + 0.161089C \\ & + 0.006974AB - 0.000059AC - 0.002533BC \\ & + 0.000018A^2 + 0.266906B^2 \\ & - 0.002429C^2 + 19.6779. \end{aligned} \tag{9}$$

$$\begin{aligned} x_5 = {} & -0.012866A - 1.3009B + 0.044038C \\ & + 0.001871AB - 0.00002AC - 0.000767BC \\ & + 4.3075 \times 10^{-6}A^2 + 0.073019B^2 \\ & - 0.000643C^2 + 5.22166. \end{aligned} \tag{10}$$

$$\begin{aligned} W = {} & 0.000449A - 0.524899B + 0.007401C \\ & + 0.000205AB - 3.57213 \times 10^{-6}AC \\ & + 0.000802BC - 2.01294 \times 10^{-6}A^2 \\ & + 0.024948B^2 - 0.000255C^2 + 2.56827. \end{aligned} \tag{11}$$

The multiple linear regression models (Eqs. 6 to 11) were evaluated using the F test, and the results are summarized in Table 5. The analysis confirms that the fitted regression models exhibit satisfactory goodness-of-fit.

To analyze the significance of the effect of each independent variable (rotational speed, grinding media size, bar spacing) on the comprehensive index of milling performance, the results of the analysis of variance (ANOVA) are shown in Table 6.

As shown in Table 6, the regression model for the comprehensive index of milling performance is highly significant ($P < 0.01$), with a correlation coefficient of $R^2 = 0.9873$, indicating a good fit of the regression equation. The ANOVA revealed that the factors influencing the comprehensive index of milling performance ranked in the following order of importance: grinding media size (B) > rotational speed (A) > bar spacing (C).

The residual analysis of the comprehensive index of milling performance is illustrated in Fig. 17. As illustrated in Fig. 17, the residuals of the comprehensive index of milling performance are randomly scattered around the reference line, with no discernible pattern, confirming that the fitted regression model achieves adequate predictive accuracy.

The response surface plots illustrating the effects of these factors on the comprehensive index of milling performance are presented in Fig. 18.

Response surface optimization was performed to maximize the comprehensive index of milling performance. With weight coefficients assigned as 0.4 for energy efficiency, 0.2 for stirrer wear, 0.2 for collision frequency, 0.1 for average normal collision force, and 0.1 for average tangential collision force, the optimal operating parameters of the rod-type stirred mill are determined as follows: a rotational speed of $398\,\mathrm{r\,min^{-1}}$, a grinding media size of 6 mm, and bar spacing of 21.2 mm. Under these conditions, the predicted comprehensive grinding performance indicator is 0.781.

To validate the accuracy of the response surface model, the optimal parameter combination (a rotational speed of $398\,\mathrm{r\,min^{-1}}$, a grinding media size of 6 mm, and bar spacing of 21.2 mm) was simulated using EDEM software. A comparison between the RSM (response surface methodology) predictions and the DEM simulation results is presented in Table 7. As shown in Table 7, the comprehensive index of milling performance obtained from the DEM simulation is 0.775, closely matching the RSM prediction of 0.781, with a relative error of only 0.77 %. These results confirm that the RSM for the comprehensive index of milling perfor-

Table 4. Experimental results.

Design point	A	B	C	$\overline{x}_{1,i}$	$\overline{x}_{2,i}$	$\overline{x}_{3,i}$	$\overline{x}_{4,i}$	$\overline{x}_{5,i}$	W_i
1	−1	−1	0	0.617	0.391	2.346	0.212	0.220	0.681
2	1	−1	0	1.042	1.031	2.323	0.458	0.460	0.767
3	−1	1	0	0.890	0.991	0.288	1.159	1.176	0.449
4	1	1	0	1.378	2.459	0.234	2.997	2.931	0.699
5	−1	0	−1	0.774	0.457	0.755	0.524	0.539	0.475
6	1	0	−1	1.266	1.319	0.669	1.250	1.247	0.626
7	−1	0	1	0.724	0.454	0.743	0.501	0.513	0.449
8	1	0	1	1.222	1.344	0.675	1.176	1.160	0.589
9	0	−1	−1	0.846	0.661	2.454	0.326	0.336	0.763
10	0	1	−1	1.150	1.751	0.263	1.949	1.946	0.552
11	0	−1	1	0.807	0.650	2.394	0.306	0.311	0.733
12	0	1	1	1.078	1.453	0.269	1.885	1.874	0.570
13	0	0	0	0.995	0.831	0.722	0.855	0.861	0.548
14	0	0	0	1.055	0.811	0.717	0.849	0.857	0.574
15	0	0	0	1.047	0.800	0.717	0.853	0.859	0.573
16	0	0	0	1.034	0.797	0.716	0.846	0.852	0.567
17	0	0	0	1.075	0.800	0.716	0.852	0.859	0.584

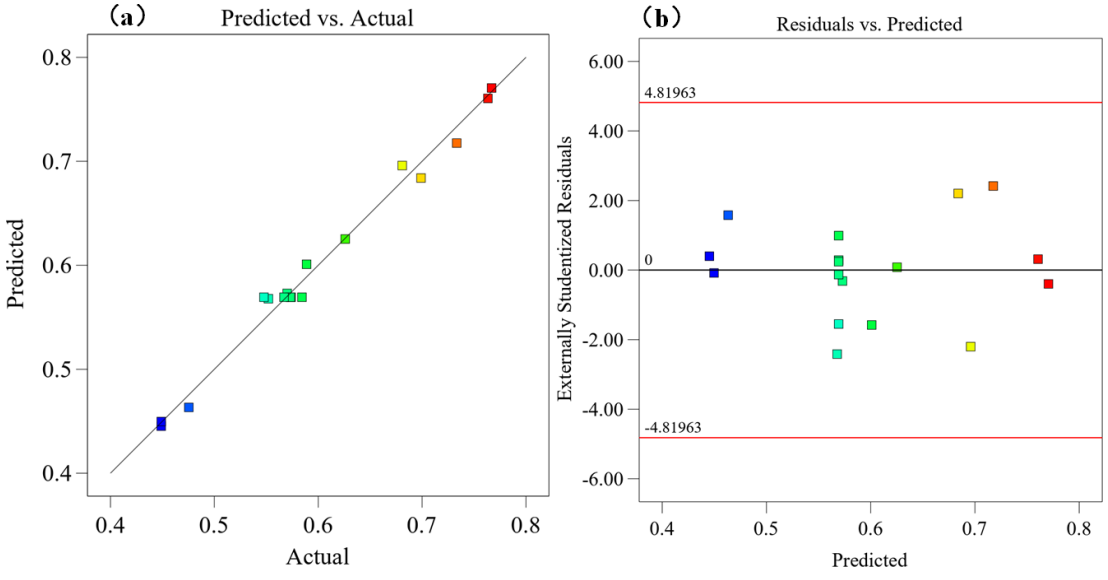

Figure 17. The residual analysis of the comprehensive index of milling performance: **(a)** comparison of predicted values with actual values and **(b)** residual plots.

mance, developed using the Box–Behnken experimental design, demonstrates high predictive accuracy.

4.4 Weight sensitivity analysis

To further validate the model, the weight coefficients associated with the comprehensive indicator were redistributed, and four weight sensitivity studies were conducted. The calculation results obtained under different weight allocations are presented in Table 8. As shown in Table 8, when the relevant weights vary, the optimal parameters for motor speed and grinding media size remain unchanged, whereas the bar spacing and the comprehensive grinding performance indicator differ. With weight coefficients assigned as 0.4 for energy efficiency, 0.2 for stirrer wear, 0.2 for collision frequency, 0.1 for average normal collision force, and 0.1 for average tangential collision force, the optimal operating parameters of the rod-type stirred mill are determined as follows: rotational speed of 398 r min^{-1}, grinding media size of 6 mm, and bar spacing of 21.2 mm. Under these conditions, the predicted comprehensive grinding performance indicator is 0.781, and

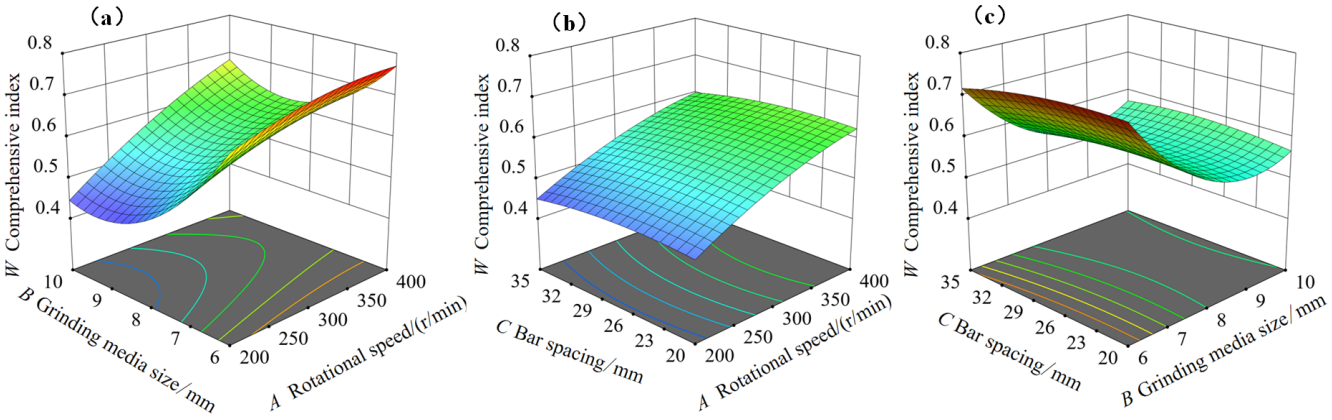

Figure 18. The effects of factors on the comprehensive index of milling performance: **(a)** influence of rotational speed and grinding media size, **(b)** influence of rotational speed and bar spacing, and **(c)** influence of grinding media size and bar spacing.

Table 5. F value of variance analysis of indices.

Norm	F value	Significance test	Significance
x_1	110.45	$F_{0.05}(9,7) = 3.677$	significant
x_2	107.46		significant
x_3	1758.87		significant
x_4	92.54		significant
x_5	101.71		significant
W	60.52		significant

the error between the DEM simulation validation results and the predicted value is only 0.77 %.

This study adopts the core methodological framework developed by Xie et al. (2024) for spiral stirred mills using DEM, which integrates comprehensive grinding performance indicators such as energy efficiency, wear, collision frequency, and normal/tangential collision forces. However, the research object is extended from a vertical spiral stirred mill to a rod stirring mill, with adaptive adjustments made to accommodate the different mill geometries (stirring rod versus helical blade). On this basis, two improvements are made to the original method. First, the orthogonal experimental design is replaced by the Box–Behnken response surface methodology, allowing a more precise non-linear regression model to be established. Second, the simulation model is validated through physical experiments (torque and power tests), achieving an error of less than 6.9 %, thereby addressing the lack of experimental validation in the spiral-type study. In summary, the contributions of this research lie primarily in extending an existing methodological framework to a new object, refining the optimization method, and supplementing experimental validation. These represent incremental progress at the level of engineering application rather than an original theoretical or methodological breakthrough.

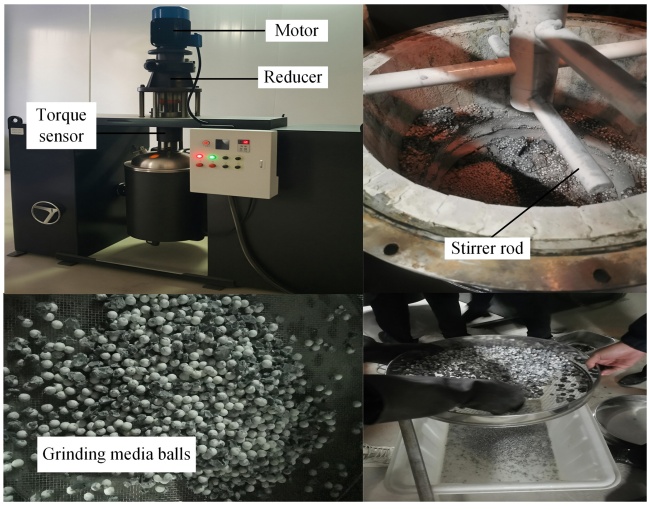

Figure 19. Grinding experiment using the rod-type stirred mill.

5 Experimental validation of the DEM model

To validate the accuracy of the DEM model proposed in this paper, an experimental setup for a rod-type stirred mill was constructed, as shown in Fig. 19.

To measure the output torque of the motor shaft, a torque sensor was installed between the reducer and the stirring rod. The motor output power was then obtained by combining the torque with the rotational speed. The comparison between the experimental torque and power values measured at different rotational speeds and the corresponding DEM simulation results is shown in Fig. 20. Figure 20 shows that, at the same rotational speed, the error between the experimental output power of the rod-type stirred mill and the DEM simulation value is within 5.3 %, and the torque error is within 6.5 %.

The comparison between the measured torque and power values obtained from experiments at different grinding media

Table 6. The ANOVA of the comprehensive index of milling performance.

Source	Sum of squares	Degrees of freedom	Mean square	F value	P value	Significance
Model	0.1573	9	0.0175	60.52	< 0.0001	**
A speed	0.0491	1	0.0491	169.95	< 0.0001	**
B media size	0.0569	1	0.0569	196.95	< 0.0001	**
C bar spacing	0.0007	1	0.0007	2.48	0.1592	
AB	0.0067	1	0.0067	23.30	0.0019	**
AC	0.0000	1	0.0000	0.0994	0.7617	
BC	0.0006	1	0.0006	2.01	0.1997	
A^2	0.0017	1	0.0017	5.91	0.0454	*
B^2	0.0419	1	0.0419	145.22	< 0.0001	**
C^2	0.0009	1	0.0009	2.99	0.1273	
Residual	0.0020	7	0.0003			
Lack of fit	0.0013	3	0.0004	2.35	0.2134	
Pure error	0.0007	4	0.0002			
Cor total	0.1593	16				
	R^2	0.9873	R^2_{adj}	0.971		

Note: ** indicates highly significant difference ($P < 0.01$); * indicates significant difference ($0.01 \le P < 0.05$).

Table 7. Comparison of the RSM predictions with the EDEM simulations.

Name	Energy efficiency (x_1)	Stirrer wear (x_2) (mm)	Collision frequency collisions/(x_3) (frequency (s))	Average normal collision force (x_4) (N)	Average tangential collision force (x_5) (N)	Comprehensive index of milling performance (W)
RSM predictions	0.15	0.0068	95137037	1.581	0.451	0.781
DEM simulations	0.151	0.007	95897107	1.632	0.466	0.775

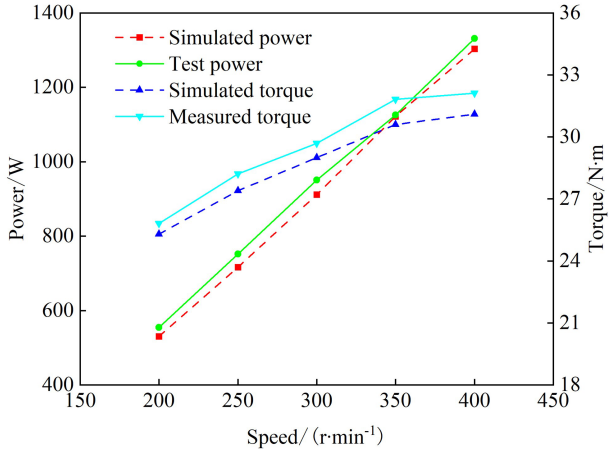

Figure 20. Measured vs. simulated torque and power at different rotational speeds.

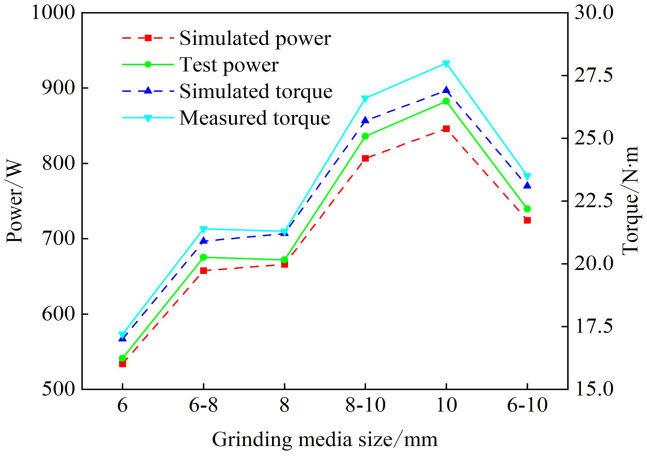

Figure 21. Measured vs. simulated torque and power at different grinding media sizes.

sizes and the corresponding DEM simulation results is shown in Fig. 21.

Figure 21 shows that, at the same grinding media size, the error between the experimental output power of the rod-type stirred mill and the DEM simulation value is within 5.6 %, and the torque error is within 6.9 %. Based on Figs. 20 and 21, the high accuracy of the established DEM model of the rod-type stirred mill was validated through torque and power experiments conducted under different rotational speeds and under different grinding media sizes.

Table 8. Optimization results obtained from the RSM model under different weights.

Name	The corresponding weights of x_1 to x_5					Optimal process parameters			
	x_1	x_2	x_3	x_4	x_5	Rotational speed ($r\,min^{-1}$)	Grinding media size (mm)	Bar spacing (mm)	Comprehensive index of milling performance (W)
Value	0.4	0.2	0.2	0.1	0.1	398	6	21.2	0.781
	0.2	0.2	0.2	0.2	0.2	398	6	26.7	0.98
	0.3	0.2	0.2	0.15	0.15	398	6	27	0.83
	0.5	0.15	0.15	0.1	0.1	398	6	26.5	0.93
	0.6	0.1	0.1	0.1	0.1	398	6	24.4	1.18

6 Conclusions

1. A simulation model of a stirred rod mill was established using the discrete element method, enabling the acquisition of grinding media velocity, stirrer pressure, and wear distribution. The effects of mill rotational speed, grinding media size, and bar spacing on grinding performance were subsequently analyzed.

2. Using rotational speed, grinding media size, and bar spacing as independent variables, a comprehensive index of milling performance was developed by incorporating energy efficiency, stirrer wear, collision frequency, and average normal and tangential collision forces. A Box–Behnken experimental design was employed, and a multiple linear regression equation for the comprehensive index of milling performance was obtained through response surface fitting. Analysis of variance was then conducted to determine the relative significance of rotational speed, grinding media size, and bar spacing on grinding performance.

3. With weight coefficients assigned as 0.4 for energy efficiency, 0.2 for stirrer wear, 0.2 for collision frequency, 0.1 for average normal collision force, and 0.1 for average tangential collision force, response surface optimization was conducted. Under the current weighting scheme, the optimal operating parameters of the rod-type stirred mill are determined as follows: a rotational speed of 398 $r\,min^{-1}$, a grinding media size of 6 mm, and bar spacing of 21.2 mm. Under these conditions, the predicted comprehensive grinding performance indicator is 0.781, and the error between the DEM simulation validation results and the predicted value is only 0.77 %. The high accuracy of the established DEM model was validated through torque and power experiments under different rotational speeds, as well as comparative torque and power experiments under different grinding media sizes.

Code availability. The present study did not involve the development of any custom software code. All numerical simulations were carried out using the commercial finite element software EDEM. No user-defined subroutines were employed in this study. The source code of EDEM is proprietary and not publicly accessible due to licensing restrictions. Therefore, no standalone software code is available for public release. The numerical procedures, material models, boundary conditions, and analysis parameters are described in sufficient detail in the paper to ensure reproducibility of the results.

Data availability. The data supporting the findings of this study are not publicly available due to confidentiality and institutional restrictions. The data are associated with ongoing research projects and therefore cannot be publicly released. However, the data may be made available from the corresponding author upon reasonable request and with permission from the relevant parties.

Author contributions. WZG proposed research approaches related to the grinding performance of rod mills. CWL conducted experimental design and data processing. CWL drafted the paper. WZG reviewed and edited the article.

Competing interests. The contact author has declared that neither of the authors has any competing interests.

Disclaimer. Publisher's note: Copernicus Publications remains neutral with regard to jurisdictional claims made in the text, published maps, institutional affiliations, or any other geographical representation in this paper. The authors bear the ultimate responsibility for providing appropriate place names. Views expressed in the text are those of the authors and do not necessarily reflect the views of the publisher.

Acknowledgements. The authors gratefully acknowledge the financial support provided by the Anhui University of Science and Technology Medical Special Cultivation Program under grant no. YZ2023H2C007.

Financial support. This research has been supported by the Anhui University of Science and Technology Medical Special Cultivation Program (grant no. YZ2023H2C007).

Review statement. This paper was edited by Zhengjian Wang and reviewed by two anonymous referees.

References

AmanNejad, M. and Barani, K.: Effects of ball size distribution and mill speed and their interactions on ball milling using DEM, Min. Proc. Ext. Met. Rev., 42, 374–379, https://doi.org/10.1080/08827508.2020.1781630, 2021.

Barrios, G. K. P., Jiménez-Herrera, N., and Tavares, L. M.: Simulation of particle bed breakage by slow compression and impact using a DEM particle replacement model, Adv. Powder Technol., 31, 2749–2758, https://doi.org/10.1016/j.apt.2020.05.011, 2020.

Bor, A., Jargalsaikhan, B., Lee, J., and Choi, H.: Effect of different milling media for surface coating on the copper powder using two kinds of ball mills with discrete element method simulation, Coatings, 10, 898, https://doi.org/10.3390/coatings10090898, 2020.

Cleary, P. W. and Owen, P.: Effect of particle shape on structure of the charge and nature of energy utilisation in a SAG mill, Miner. Eng., 132, 48–68, https://doi.org/10.1016/j.mineng.2018.12.006, 2019.

Daraio, D., Villoria, J., Ingram, A., Alexiadis, A., Stitt, E. H., and Marigo, M.: Investigating grinding media dynamics inside a vertical stirred mill using the discrete element method: Effect of impeller arm length, Powder Technol., 364, 1049–1061, https://doi.org/10.1016/j.powtec.2019.09.038, 2020.

De Oliveira, A. L. R., De Carvalho, R. M., and Tavares, L. M.: Predicting the effect of operating and design variables in grinding in a vertical stirred mill using a mechanistic mill model, Powder Technol., 387, 560–574, https://doi.org/10.1016/j.powtec.2021.04.057, 2021.

Ding, W., Li, Z., Zeng, Y., Wang, G., and Guan, W.: Analysis of collision energy of semi-autogenous mills with different ore grades based on DEM-CFD, Journal of Central South University, Sci. Technology, 56, 2149–2156, https://doi.org/10.11817/j.issn.1672-7207.2025.06.001, 2025.

Fukui, S., Tsunazawa, Y., Hisatomi, S., and Sekiguchi, T.: Effect of agitator shaft direction on grinding performance in media stirred mill: Investigation using DEM simulation, Mater. Trans., 59, 488–493, https://doi.org/10.2320/matertrans.M-M2017855, 2018.

Govender, N., Rajamani, R., Wilke, D. N., Wu, C. Y., Khinast, J., and Glasser, B. J.: Effect of particle shape in grinding mills using a GPU based DEM code, Miner. Eng., 129, 71–84, https://doi.org/10.1016/j.mineng.2018.09.019, 2018.

Kumar, A., Sahu, R., and Tripathy, S. K.: Energy-efficient advanced ultrafine grinding of particles using stirred mills – a review, Energies, 16, 5277, https://doi.org/10.3390/en16145277, 2023.

Kumar, M., Xiong, X., Wan, Z., Sun, Y., Tsang, D. C. W., and Gupta, J.: Ball milling as a mechanochemical technology for fabrication of novel biochar nanomaterials, Bioresource Technol., 312, 123613, https://doi.org/10.1016/j.biortech.2020.123613, 2020.

Liu, Z., Wang, G., Guan, W., Sun, G., and Chen, Z.: Research on performance of a laboratory-scale SAG mill based on DEM-EMBD, Powder Technol., 406, 117581, https://doi.org/10.1016/j.powtec.2022.117581, 2022.

Miao, Q., Huang, P., and Zhu, W.: Morphology of impact fragmentation distribution of single spherical and ellipsoidal particles in drop weight experiments, Particuology, 86, 137–148, https://doi.org/10.1016/j.partic.2023.05.004, 2024.

Mittal, A., Kumar, M., and Mangadoddy, N.: A coupled CFD–DEM model for tumbling mill dynamics – effect of lifter profile, Powder Technol., 433, 119178, https://doi.org/10.1016/j.powtec.2023.119178, 2024.

Oliveira, A. L. R., Rodriguez, V. A., De Carvalho, R. M., Powell, M., and Tavares, L. M.: Mechanistic modeling and simulation of a batch vertical stirred mill, Miner. Eng., 156, 106487, https://doi.org/10.1016/j.mineng.2020.106487, 2020.

Ou, T., Liu, J., and Chen, W.: A coupled discrete element modelling and smoothed particle hydrodynamics method and applications, Journal of Hunan University (Natural Sciences), 50, 187–193, https://doi.org/10.16339/j.cnki.hdxbzkb.2023193, 2023.

Prziwara, P., Hamilton, L. D., Breitung-Faes, S., and Kwade, A.: Impact of grinding aids and process parameters on dry stirred media milling, Powder Technol., 335, 114–123, https://doi.org/10.1016/j.powtec.2018.05.021, 2018.

Tavares, L. M. and Das Chagas, A. S.: A stochastic particle replacement strategy for simulating breakage in DEM, Powder Technol., 377, 222–232, https://doi.org/10.1016/j.powtec.2020.08.091, 2021.

Xie, C., Zhao, Y., Song, T., and Zhao, Y.: Investigation of the effect of filling level on the wear and vibration of a SAG mill by DEM, Particuology, 63, 24–34, https://doi.org/10.1016/j.partic.2021.04.009, 2022.

Xie, P., Cui, D., Wang, G., and Li, K.: Working performance of vertical screw stirring mill based on discrete element method, Journal of Jilin University (Engineering and Technology Edition), 54, 2423–2431, https://doi.org/10.13229/j.cnki.jdxbgxb.20221424, 2024.